Available online at www.eccomasproceedia.org
Eccomas Proceedia SMART (2023) 1938-1949

ECCOMAS
Proceedia

X ECCOMAS Thematic Conference on Smart Structures and Materials
SMART 2023
D.A. Saravanos, A. Benjeddou, N. Chrysochoidis and T. Theodosiou (Eds)

THERMODYNAMICALLY CONSISTENT MODELLING OF DIELECTRIC VISCOELASTIC SOLIDS UNDER FINITE STRAIN

M. Kunzemann[a,*], **A. Pechstein**[a], **A. Humer**[a]

[a] Institute of Technical Mechanics, Johannes Kepler University Linz, Austria

*Corresponding author e-mail: mario.kunzemann@jku.at

Abstract. High flexibility and excellent damping properties are characteristics of silicone-based polymers that are of interest in applications. In the current contribution, electric actuation of these materials through their dielectric properties is analyzed. The main emphasis is on estimating the effects of electric loading on the viscosity in a large deformation regime. A thermodynamically consistent material model is presented, in which free energy density and dissipation function determine elastic and electric behavior as well as the electromechanic coupling and viscous effects. A finite element formulation for the coupled problem in radially symmetric settings is developed. Two computational examples, electric actuation of a circular disc and a ball drop test, are chosen with a view to verification of the formulation though subsequent measurements.

Key words: electromechanical coupling, electro-active polymers, viscoelasticity

1 INTRODUCTION

Materials that react to non-mechanical stimuli by mechanic deformation are often consideres as *smart materials*. In engineering applications, piezoceramics probably are most prominent in the design of electromechanic actuators or sensors. Linear material models going back to Voigt [1] allow to compute small but highly accurate deformations.

More recently, soft polymers have been analyzed with respect to their electromechanic coupling properties. In dielectric media, ponderomotive forces lead to large deformations induced by an external electric field. In contrast to piezoceramics, many of these polymers are well-known for their damping properties, while they are capable of undergoing large strains of up to 100%. To adjust damping properties through electric actuation, understanding the electro-viscoelastic coupling behavior is a prerogative.

Concerning the basics on modeling large-deformation electro-elastic materials, we cite the monograph by Maugin [2], or the more recent review by Dorfmann and Ogden [3]. Ask et al. [4] provided a model for electrostrictive viscoelastic polymers at finite strains. Miehe et al. [5] discuss the modeling of dissipative effects in smart materials in a variational framework.

Peer-review under responsibility of the organizing committee of SMART 2023.
doi: 10.7712/150123.9963.450563

Based on these ideas, a thermodynamically consistent model for dielectric viscoelastic solids is developed in the current manuscript. This model is defined not only through hyperelastic and dielectric free energy densities, but also through a dissipation function to model viscoelastic losses.

As the material model is developed within a variational framework, it directly induces the definition of a finite element discretization. Having verification of our model against measurements in mind, a finite element formulation for rotationally symmetric problems is designed. This allows not only the simulation of the electric actuation of a viscoelastic disc, but also computational models of a ball drop test. Similar tests have been already been used to characterize damping properties of various polydimethylsiloxane in [6, 7], and an extension to electrically actuated specimen is of interest.

The remainder of this paper is organized as follows: Section 2 presents a thermodynamically consistent material model based on the free energy and a dissipation function. In Section 3 D'Alembert's principle is deduced from an incremental minimization problem. This directly leads to the definition of a finite element model in Section 4. Finally, in Section 5 computational results are presented.

2 A THERMODYNAMICALLY CONSISTENT MATERIAL MODEL

2.1 Kinematics

We consider a body $\mathcal{B}$ consisting of viscoelastic, dielectric material. Each material point $\mathcal{P}$ is identified by its position vector $\boldsymbol{X}$ in the reference configuration. The motion of the body is described by a time-dependent mapping $\boldsymbol{\chi}$, which maps each material point to its current spatial position at time t, $\boldsymbol{x} = \boldsymbol{\chi}(\boldsymbol{X}, t)$. We use standard notations for all relevant kinematic quantities, starting with the displacement field $\boldsymbol{u} = \boldsymbol{x} - \boldsymbol{X}$. Throughout the following, we identify derivatives of fields with respect to reference coordinates $\boldsymbol{X}$ by using capital operators. Derivatives with respect to spatial coordinates $\boldsymbol{x}$ are identified using lower case operators. The deformation gradient is then defined as $\mathbf{F} = \operatorname{Grad} \boldsymbol{\chi} = \mathbf{I} + \operatorname{Grad} \boldsymbol{u}$. As we consider incompressible elastomers in our models, a splitting of the deformation gradient into its volumetric and isochoric components is adopted, with a hat denoting the isochoric part $\mathbf{F} = J^{1/3}\hat{\mathbf{F}}$ with $J = \det \mathbf{F}$. Based on the above definitions, the right Cauchy-Green tensor $\mathbf{C}$, isochoric component of the right Cauchy-Green tensor $\hat{\mathbf{C}}$and Green's strain tensor $\mathbf{E}$ are given by

$$\mathbf{C} = \mathbf{F}^\top \cdot \mathbf{F}, \qquad \hat{\mathbf{C}} = \hat{\mathbf{F}}^\top \cdot \hat{\mathbf{F}} = J^{-2/3}\mathbf{C}, \qquad \mathbf{E} = \frac{1}{2}(\mathbf{C} - \mathbf{I}). \tag{1}$$

For incompressible materials, we have $J \equiv 1$ and $\hat{\mathbf{F}} \equiv \mathbf{F}$ as well as $\hat{\mathbf{C}} \equiv \mathbf{C}$. For modeling large deformation viscoelasticity, an extension of the one-dimensional rheological standard solid model [8] is proposed. In the standard solid model, a spring and N spring-dashpot combinations are connected in parallel. At large deformations, as an extension of the linear model, N independent stress-free *intermediate* configurations are postulated, to which the respective elastic material laws can be applied. For each of these configurations, the isochoric part of the

deformation gradient decomposes multiplicatively into an elastic part $\hat{\mathbf{F}}_{e,i}$ and a viscoelastic part $\mathbf{F}_{v,i}$, see, e.g., [4]

$$\hat{\mathbf{F}} = \hat{\mathbf{F}}_{e,i} \cdot \mathbf{F}_{v,i}, \text{ for } i \in \{1, \dots N\}. \tag{2}$$

Above, the viscoelastic parts $\mathbf{F}_{v,i}$ of the deformation resemble the transformation the stress-free i^{th} intermediate configuration, where $\mathbf{F}_{v,i}$ is not necessarily compatible. However, it is assumed that the viscoelastic contributions are modeled in an isochoric way, such that $J_{v,i} = \det \mathbf{F}_{v,i} \equiv 1$ for all $i = 1 \dots N$. Based on the i^{th} elastic isochoric part of the deformation gradient $\hat{\mathbf{F}}_{e,i} = \hat{\mathbf{F}} \cdot \mathbf{F}_{v,i}^{-1}$, the corresponding elastic and viscoelastic Cauchy-Green tensors can be defined via

$$\hat{\mathbf{C}}_{e,i} = \hat{\mathbf{F}}_{e,i}^{\top} \cdot \hat{\mathbf{F}}_{e,i} = \mathbf{F}_{v,i}^{-\top} \cdot \hat{\mathbf{C}} \cdot \mathbf{F}_{v,i}^{-1}, \qquad \mathbf{C}_{v,i} = \mathbf{F}_{v,i}^{\top} \cdot \mathbf{F}_{v,i}. \tag{3}$$

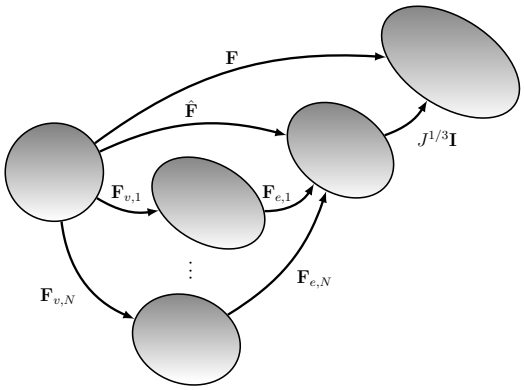

Figure 1: Representation of the mulitplicative decomposition

2.2 Large deformation electrostatics

As common in the simulation of electroactive materials, we assume that the material is non-conducting and we remain in the electrostatic regime. Electric field $\boldsymbol{e}$ and dielectric displacement $\boldsymbol{d}$ are defined in spatial configuration. From Faraday's law $\operatorname{curl} \boldsymbol{e} = 0$ on a simply connected domain, one can deduce that the electric field is a gradient field $\boldsymbol{e} = -\operatorname{grad} \phi$, where ϕ describes the electric potential. Furthermore, as there are no free charges in non-conducting materials, Gauss' law ensures that $\boldsymbol{d}$ is divergence free with respect to spatial coordinates.

Both electric field and dielectric displacement have material counterparts, which can be found through appropriate pull-back operations. Using capital letter for fields associated to the material configuration, one introduces

$$\boldsymbol{E} = \mathbf{F}^{\top} \cdot \boldsymbol{e} = -\operatorname{Grad} \phi, \qquad \boldsymbol{D} = J\mathbf{F}^{-1} \cdot \boldsymbol{d}. \tag{4}$$

2.3 Constitutive equations

In the following, a thermodynamically consistent model for the electroactive viscoelastic material shall be developed. To this end, the free energy density Ψ shall be defined for independent Cauchy-Green tensor $\mathbf{C}$ or deformation gradient $\mathbf{F}$ and electric field $\boldsymbol{E}$. The viscoelastic

Cauchy-Green tensors $\mathbf{C}_{v,i}$ will serve as internal variables, and pressure p will act as a Lagrangian multiplier for the incompressibility constraint.

The free energy is assumed to be additively composed of several independent potentials, compare [4]. We consider a decomposition into a hyperelastic potential Ψ_∞, viscoelastic energy densities $\Psi_{v,i}$, and an electric energy Ψ_{el}, which shall be defined in turn throughout the following sections,

$$\Psi(\mathbf{C}, \mathbf{C}_{v,i}, p, \boldsymbol{E}) = \Psi_\infty(\mathbf{C}, p) + \sum_{i=1}^{N} \Psi_{v,i}(\hat{\mathbf{C}}, \mathbf{C}_{v,i}) + \Psi_{el}(\mathbf{C}, \boldsymbol{E}). \tag{5}$$

To account for the effects of vacuum, we rather consider the *augmented free energy density*,

$$\Omega(\mathbf{C}, \mathbf{C}_{v,i}, p, \boldsymbol{E}) = \Psi - \frac{1}{2}\epsilon_0 J \boldsymbol{E} \cdot \mathbf{C}^{-1} \cdot \boldsymbol{E}. \tag{6}$$

The Clausius-Duhem inequality states essentially that dissipation $\mathcal{D}$ is non-negative(cf. [9]),

$$\mathcal{D} = \frac{1}{2}\mathbf{T} : \dot{\mathbf{C}} - \boldsymbol{D} \cdot \dot{\boldsymbol{E}} - \dot{\Omega} \geq 0. \tag{7}$$

Above, $\mathbf{T}$ is the total second Piola-Kirchhoff stress. Computing the rate $\dot{\Omega}$ explicitely, (7) becomes

$$\mathcal{D} = -\left(\frac{\partial \Omega}{\partial \mathbf{C}} - \frac{1}{2}\mathbf{T}\right) : \dot{\mathbf{C}} - \left(\frac{\partial \Omega}{\partial \boldsymbol{E}} + \boldsymbol{D}\right) : \dot{\boldsymbol{E}} - \sum_{i=1}^{N} \frac{\partial \Omega}{\partial \mathbf{C}_{v,i}} : \dot{\mathbf{C}}_{v,i} - \frac{\partial \Omega}{\partial p}\dot{p} \geq 0. \tag{8}$$

Eq. (8) implies the classical constitutive equations for the total second Piola-Kirchhoff stress $\mathbf{T}$ and the dielectric displacement vector $\boldsymbol{D}$ as

$$\mathbf{T} = 2\frac{\partial \Omega}{\partial \mathbf{C}}, \qquad\qquad \boldsymbol{D} = -\frac{\partial \Omega}{\partial \boldsymbol{E}}. \tag{9}$$

Moreover, pressure p acting as a Lagrangian multiplier ensures the condition of incompressibility as $\partial\Omega/\partial p = 0$. The reduced dissipation inequality states that the negative inner product of *generalized driving forces* $\partial\Omega/\partial\mathbf{C}_{v,i}$ and viscous strain rates $\dot{\mathbf{C}}_{v,i}$ is non-negative,

$$\mathcal{D} = -\sum_{i=1}^{N} \frac{\partial \Psi}{\partial \mathbf{C}_{v,i}} : \dot{\mathbf{C}}_{v,i} \geq 0. \tag{10}$$

Free energy Let us collect specific representations for the energy densities constituting the augmented free energy Ω. The elastic part of the free energy Ψ_∞ will be governed by an incompressible Neo-Hookean hyperelastic potential. We use $\mu_\infty = G_\infty$ for the long-term shear modulus,

$$\Psi_\infty(\mathbf{C}, p) = \frac{\mu_\infty}{2}\left(\operatorname{tr}\hat{\mathbf{C}} - 3\right) - p \log J. \tag{11}$$

The hydrostatic pressure p serves as a Lagrangian multiplier to ensure the incompressibility constraint $\partial\Psi_\infty/\partial p = \log J = 0$, such that $J \equiv 1$.

Concerning the i^{th} multiplicative decomposition, a similar incompressible Neo-Hookean hyperelastic potential models the elastic energy for $\hat{\mathbf{C}}_{e,i}$ with shear modulus $\mu_{v,i}$. As $\operatorname{tr}\hat{\mathbf{C}}_{e,i} = \hat{\mathbf{C}} : \mathbf{C}_{v,i}^{-1}$, we use the representation

$$\Psi_{v,i}(\hat{\mathbf{C}}, \mathbf{C}_{v,i}) = \frac{\mu_{v,i}}{2}\left(\hat{\mathbf{C}} : \mathbf{C}_{v,i}^{-1} - 3\right). \tag{12}$$

The electric contribution Ψ_{el} models polarization of the material. For an isotropic linear dielectric, it is defined through the material electric susceptibility $\chi = \epsilon_r - 1$ and vacuum permittivity ϵ_0 . As the augmented free energy Ω includes vacuum effects, it proves useful to directly define the *augmented electric energy density* Ψ_{el}^{aug}, which is enriched accordingly,

$$\Psi_{el}^{aug}(\mathbf{C}, \boldsymbol{E}) = -\frac{1}{2}\epsilon_0(\chi + 1)\boldsymbol{E} \cdot \mathbf{C}^{-1} \cdot \boldsymbol{E}. \tag{13}$$

Dissipation Viscoelastic evolution is defined implicitly through a *dissipation function* Φ such that

$$\mathcal{D} = \sum_{i=1}^{N} \frac{\partial \Phi}{\partial \dot{\mathbf{C}}_{v,i}} : \dot{\mathbf{C}}_{v,i}. \tag{14}$$

As for the free energy densities, we also assume the dissipation function to be composed additively from contributions due to the N internal variables $\mathbf{C}_{v,i}$. Each of the terms is governed by a viscosity parameter η_i. To be specific, we use

$$\Phi = \sum_{i=1}^{N} \Phi_i(\mathbf{C}_{v,i}, \dot{\mathbf{C}}_{v,i}), \qquad \Phi_i(\mathbf{C}_{v,i}, \dot{\mathbf{C}}_{v,i}) = \frac{1}{12}\sum_{i=1}^{N} \eta_i(\mathbf{C}_{v,i}^{-1} \cdot \dot{\mathbf{C}}_{v,i}) : (\mathbf{C}_{v,i}^{-1} \cdot \dot{\mathbf{C}}_{v,i}). \tag{15}$$

The implication of this choice on the evolution of $\mathbf{C}_{v,i}$ is discussed in Section 3.

3 INCREMENTAL MINIMIZATION PRINCIPLE

We deduce a variational formulation for electro-viscoelastic solids defining an incremental minimization problem. A similar procedure was presented for electro-magneto-mechanically coupled problems by Miehe et al. [5]. For reasons of simplicity of presentation, we restrict ourselves to the case of a conservative volume force density $\boldsymbol{f}$. With ρ the mass density we get the kinetic energy $T = 1/2\rho\dot{\boldsymbol{u}} \cdot \dot{\boldsymbol{u}}$ and power of external forces $\mathcal{P}_{ext} = \boldsymbol{f} \cdot \dot{\boldsymbol{u}}$. Consider a finite time step $[t_0, t_0 + \Delta t]$ with known initial conditions at time t_0. We introduce the *incremental potential* for this time step as

$$\Pi_t^{t+\Delta t} = \int_{t_0}^{t_0+\Delta t} (\dot{T} + \dot{\Omega} + \Phi - \mathcal{P}_{ext})\, dt \tag{16}$$

$$= \underbrace{T_{t_0+\Delta t} - T_{t_0}}_{kinetic} + \underbrace{\Omega_{t_0+\Delta t} - \Omega_{t_0}}_{\text{stored}} + \underbrace{\int_{t_0}^{t_0+\Delta t} \Phi dt}_{\text{dissipated}} - \underbrace{\int_{t_0}^{t_0+\Delta t} \mathcal{P}_{ext}\, dt}_{\text{external}}. \tag{17}$$

The incremental potential $\Pi_{t_0}^{t_0+\Delta t}$ is then minimized with respect to all admissible displacement functions and the viscoelastic internal parameters, and maximized with respect to the electric potential (or electric field) and pressure. For time step size Δt approaching zero, we arrive at

$$\dot{T} + \dot{\Omega} + \Phi - \mathcal{P}_{ext} \to \min_{\dot{\mathbf{C}}} \min_{\dot{\mathbf{C}}_{v,i}} \max_{\dot{E}} \max_{\dot{p}}. \tag{18}$$

We can now rewrite Eq.(18) for the specific choice of augmented free energy Ω and get,

$$\rho\ddot{\boldsymbol{u}} \cdot \dot{\boldsymbol{u}} + \frac{\partial \Omega}{\partial \mathbf{C}} : \dot{\mathbf{C}} + \sum_{i=1}^{N} \frac{\partial \Omega}{\partial \mathbf{C}_{v,i}} : \dot{\mathbf{C}}_{v,i} + \frac{\partial \Omega}{\partial \boldsymbol{E}} \cdot \dot{\boldsymbol{E}} + \frac{\partial \Omega}{\partial p}\dot{p} + \Phi - \boldsymbol{f} \cdot \dot{\boldsymbol{u}} \to \min_{\dot{\mathbf{C}},\, \dot{\mathbf{C}}_{v,i}} \max_{\dot{E},\, \dot{p}} \tag{19}$$

As the dissipation function Φ is smooth, the optimization problem is equivalent to finding critical points as solutions to the corresponding variational equation, also known as D'Alembert's principle,

$$\begin{aligned} \int_{\mathcal{B}} \rho\ddot{\boldsymbol{u}} \cdot \delta\boldsymbol{u}\, dV + \int_{\mathcal{B}} \left(\frac{\partial \Omega}{\partial \mathbf{C}} : \delta\mathbf{C} + \sum_{i=1}^{N} \frac{\partial \Omega}{\partial \mathbf{C}_{v,i}} : \delta\mathbf{C}_{v,i} + \frac{\partial \Omega}{\partial \boldsymbol{E}} \cdot \delta\boldsymbol{E} + \frac{\partial \Omega}{\partial p}\delta p \right) dV \\ + \int_{\mathcal{B}} \sum_{i=1}^{N} \frac{\partial \Phi}{\partial \dot{\mathbf{C}}_{v,i}} : \delta\mathbf{C}_{v,i}\, dV - \int_{\mathcal{B}} \boldsymbol{f} \cdot \delta\boldsymbol{u}\, dV = 0. \end{aligned} \tag{20}$$

For a simplified presentation, we rewrite D'Alembert's principle in more compact form, although abusing notation concerning the variation of the dissipation function,

$$\int_{\mathcal{B}} \left(\rho\ddot{\boldsymbol{u}} \cdot \delta\boldsymbol{u} + \delta\Omega + \delta\Phi - \boldsymbol{f} \cdot \delta\boldsymbol{u} \right) dV = 0, \qquad \text{with } \delta\Phi := \sum_{i=1}^{N} \frac{\partial \Phi}{\partial \dot{\mathbf{C}}_{v,i}} : \delta\mathbf{C}_{v,i}. \tag{21}$$

The variational equation (20) implicitly defines the evolution law for $\dot{\mathbf{C}}_{v,i}$ for arbitrary but fixed index $i \in \{1, \dots N\}$. We show that, for the proposed choice of dissipation function from (15), the standard model as e.g. proposed by [8] is reestablished. We collect all terms containing $\delta\mathbf{C}_{v,i}$ from Eq.(20), and obtain,

$$\int_{\mathcal{B}} \left(\frac{\partial \Psi_{v,i}}{\partial \mathbf{C}_{v,i}} + \frac{1}{6}\eta_i \left(\mathbf{C}_{v,i}^{-1} \cdot \dot{\mathbf{C}}_{v,i} \cdot \mathbf{C}_{v,i}^{-1} \right) \right) : \delta\mathbf{C}_{v,i}\, dV = 0. \tag{22}$$

Since $\det \mathbf{C}_{v,i} = 1$, we observe for its rate and variation,

$$\frac{d}{dt}(\det \mathbf{C}_{v,i}) = \mathbf{C}_{v,i}^{-1} : \dot{\mathbf{C}}_{v,i} = 0, \qquad \delta(\det \mathbf{C}_{v,i}) = \mathbf{C}_{v,i}^{-1} : \delta\mathbf{C}_{v,i} = 0. \tag{23}$$

Thus, a contribution of the form $\alpha {\mathbf{C}_{v,i}}^{-1} : \delta\mathbf{C}_{v,i} = 0$ can be added to Eq.(22) leading to,

$$\int_{\mathcal{B}} \left(\frac{\partial \Psi_{v,i}}{\partial \mathbf{C}_{v,i}} + \alpha\mathbf{C}_{v,i}^{-1} + \frac{1}{6}\eta_i \mathbf{C}_{v,i}^{-1} \cdot \dot{\mathbf{C}}_{v,i} \cdot \mathbf{C}_{v,i}^{-1} \right) : \delta\mathbf{C}_{v,i}\, dV = 0. \tag{24}$$

As $\delta\mathbf{C}_{v,i}$ is otherwise arbitrary, the equality holds in classical sense. Introducing Mandel-type stress tensors $\mathbf{M}_{v,i} = -\mathbf{C}_{v,i} \cdot \partial\Psi_{v,i}/\partial\mathbf{C}_{v,i}$, we observe after some algebraic manipulations,

$$\eta_i \dot{\mathbf{C}}_{v,i} = 6\,(\mathbf{M}_{v,i} - \alpha\mathbf{I}) \cdot \mathbf{C}_{v,i}. \tag{25}$$

Recall that in Eq. (23) states that ${\mathbf{C}_{v,i}}^{-1} \colon \dot{\mathbf{C}}_{v,i}$ must vanish, which can be used to determine the unknown parameter α through

$$0 = \eta_i \mathbf{C}_{v,i}^{-1} \colon \dot{\mathbf{C}}_{v,i} = 6\,(\mathbf{M}_{v,i} - \alpha\mathbf{I}) : \mathbf{I}. \tag{26}$$

Eq. (26) directly implies $\alpha = 1/3\,\mathrm{tr}\,\mathbf{M}_{v,i}$

$$\eta_i \dot{\mathbf{C}}_{v,i} = 6\,\mathrm{dev}(\mathbf{M}_{v,i}) \cdot \mathbf{C}_{v,i}, \tag{27}$$

which is stated in similar form by [4]. To compare the final evolution law to standard theory, we explicitely compute the Mandel-type stresses for the viscoelastic potential $\Psi_{v,i}$ from (12),

$$\mathbf{M}_{v,i} = -\frac{\mu_{v,i}}{2}\left(\hat{\mathbf{C}} \cdot \mathbf{C}_{v,i}^{-1}\right). \tag{28}$$

After combining the two equations Eq. (27) and Eq. (28) we obtain the evolution law for $\mathbf{C}_{v,i}$ as stated in [8],

$$\frac{2}{3}\eta \dot{\mathbf{C}}_{v,i} = 2\mu_{v,i}\left(\hat{\mathbf{C}} - \frac{1}{3}\,\mathrm{tr}\left(\hat{\mathbf{C}} \cdot \mathbf{C}_{v,i}^{-1}\right)\mathbf{C}_{v,i}\right), \tag{29}$$

4 COMPUTATIONAL IMPLEMENTATION

We propose a computationally efficient finite element model of the above description for radially symmetric problems. This setup is designed as such as it allows for verification against various measurement setups, including classical dynamic mechanical analysis, electric actuation of a cylindric specimen as well as ball drop tests to determine rebound resiliences.

4.1 Spatial discretization for radially symmetric problems

Let the body $\mathcal{B}$ as well as all external forces and kinematic constraints be in accordance with radial symmetry. Without restriction of generality, we consider $\boldsymbol{e}_z$ as axis of rotation. Deformation gradient $\mathbf{F}$ and right Cauchy-Green tensor are defined in the standard way, assuming that the solution is independent of the angular coordinate φ.

Assume $\mathcal{T} = \{T\}$ to be a triangular finite element mesh of the section of $\mathcal{B}$ under consideration. Concerning the elastic problem, we propose to use the pair of displacement-pressure elements as proposed by Taylor and Hood [10], where both $\boldsymbol{u}$ and p are represented by continuous basis functions $\boldsymbol{N}_i^{(u)}$ and $N_i^{(p)}$ respectively, and the approximation order for $\boldsymbol{u}$ is one higher than for p. As common in electrostatic problems, the electric potential is discretized by continuous basis functions of the same order as the displacement vector. Additionally, kinematic

boundary conditions $\boldsymbol{u} = \mathbf{0}$ on the boundary part Γ_{fix} as well as $\phi = \phi_0$ on the electroded boundary Γ_{el} have to be satisfied. Summing up, finite element approximations for $\boldsymbol{u}$, p and ϕ satisfy

$$\boldsymbol{u} \in \{\boldsymbol{v} : \boldsymbol{v}|_T \in (P^k(T))^2, \boldsymbol{v} \text{ cont.}, \boldsymbol{v}|_{\Gamma_{fix}} = \mathbf{0}\}, \qquad \boldsymbol{u} = \sum_{i=1}^{n_u} q_i^{(u)} \boldsymbol{N}_i^{(u)}, \tag{30}$$

$$p \in \{q : q|_T \in P^{k-1}(T), q \text{ cont.}\}, \qquad p = \sum_{i=1}^{n_p} q_i^{(p)} N_i^{(p)}, \tag{31}$$

$$\phi \in \{\psi : \psi|_T \in P^k(T), \psi \text{ cont.}, \psi|_{\Gamma_{el}} = \phi_0\}, \qquad \phi = \sum_{i=1}^{n_\phi} q_i^{(\phi)} N_i^{(\phi)}. \tag{32}$$

Last, it is necessary to provide a finite-dimensional approximation for the viscoelastic internal variables $\mathbf{C}_{v,i}$. Here, it is important that the kinematic constraint of incompressibility is satisfied by construction. For a rotationally symmetric setting, this can be achieved by a nonlinear representation of $\mathbf{C}_{v,i}$ in terms of the independent viscoelastic strains $s_{i,rr}$, $s_{i,zz}$ and $s_{i,rz}$. The i^{th} viscoelastic Cauchy-Green tensor respects the axisymmetric structure,

$$\mathbf{C}_{v,i} = \begin{bmatrix} 2s_{i,rr}+1 & 0 & 2s_{i,rz} \\ 0 & c_{i,\varphi\varphi} & 0 \\ 2s_{i,rz} & 0 & 2s_{i,zz}+1 \end{bmatrix}. \tag{33}$$

Component $c_{i,\varphi\varphi}$ is chosen such that the incompressibility constraint $\det \mathbf{C}_{v,i} \equiv 1$ is satisfied a-priorily, which implies

$$c_{i,\varphi\varphi} = \left((2s_{i,rr}+1)(1+2s_{i,zz}) - 4s_{i,rz}\right)^{-1}. \tag{34}$$

The viscoelastic strains $s_{i,rr}, s_{i,zz}$ and $s_{i,rz}$ are defined elementwise polynomial, without continuity, one polynomial order lower than the displacements,

$$s_{i,rr}, s_{i,zz}, s_{i,rz} \in \{s : s|_T \in P^{k-1}(T)\}, \qquad s_{i,\alpha\beta} = \sum_{i=1}^{n_s} q_i^{(s,\alpha\beta)} N_i^{(s)}. \tag{35}$$

4.2 Time integration

Introducing the finite element discretizations (30), (31), (32) and (35) in D'Alembert's principle (20) leads to a system of ordinary differential equations for the degree of freedom vector $\boldsymbol{q}$. As the physical problem includes accelerations $\ddot{\boldsymbol{u}}$ and viscoelastic strain rates $\dot{\mathbf{C}}_{v,i}$, the electrostatic potential ϕ as well as Lagrangian multiplier p, a differential-algebraic system of equations is generated after spatial discretization. It is well known that the Newmark-β-scheme is well-suited to solve differential-algebraic equations of index 2, where the choice of parameter β further determines its numerical damping properties.

We shortly present the Newmark-β-scheme adapted for the viscoelastic problem at hand. To this end, we assume that velocities $\boldsymbol{v} = \dot{\boldsymbol{u}}$ are approximated by an independent linear combination of displacement basis functions $\boldsymbol{N}_i^{(u)}$, via additional degrees of freedom $q_i^{(v)}$. For any time step $[t_n, t_{n+1} = t_n + \Delta t]$, the quantities $\boldsymbol{u}_n$, $\boldsymbol{v}_n$, p_n as well as $\mathbf{C}_{v,i,n}$, $\dot{\mathbf{C}}_{v_n}$ (or rather the viscoelastic strains $s_{i,\alpha\beta,n}$ and strain rates $\dot{s}_{i,\alpha\beta,n}$) at time t_n are assumed to be available from the previous step. According updates $\boldsymbol{u}$, $\boldsymbol{v}$, p, $s_{i,\alpha\beta}$, and $s_{i,\alpha\beta}$ at time $t_{n+1} = t_n + \Delta t$ are to be computed, where we omit $n+1$ as an index in favor of brevity of presentation. The Newmark scheme interpreted in terms of the underlying variational equations leads to the coupled non-linear system, where we use $\delta\boldsymbol{v}$ as the (independent) variation of the velocity $\boldsymbol{v}$,

$$\begin{aligned}
&\int_{\mathcal{B}} \rho\,(\boldsymbol{u} - \boldsymbol{u}_n - \Delta t\,\boldsymbol{v}_n)\cdot\delta\boldsymbol{u}\,dV + \\
&\quad (\Delta t)^2 \int_{\mathcal{B}} \left(\beta(\delta\Omega + \delta\Phi - \boldsymbol{f}\cdot\delta\boldsymbol{u}) + \left(\tfrac{1}{2} - \beta\right)(\delta\Omega_n + \delta\Phi_n - \boldsymbol{f}_n\cdot\delta\boldsymbol{u})\right) dV = 0, \qquad (36)\\
&\int_{\mathcal{B}} \rho\,(\boldsymbol{v} - \boldsymbol{v}_n)\cdot\delta\boldsymbol{v}\,dV + \\
&\quad \Delta t \int_{\mathcal{B}} \left(\gamma\left(\left.\frac{\partial\Omega}{\partial\boldsymbol{u}}\right|_{t_{n+1}}\cdot\delta\boldsymbol{v} - \boldsymbol{f}\cdot\delta\boldsymbol{v}\right) + (1-\gamma)\left(\left.\frac{\partial\Omega}{\partial\boldsymbol{u}}\right|_{t_n}\cdot\delta\boldsymbol{v} - \boldsymbol{f}_n\cdot\delta\boldsymbol{v}\right)\right) dV. \qquad (37)
\end{aligned}$$

Note that equation (36) does not only implement the Newmark integration scheme for the displacements, but also the incompressibility constraint via $\partial\Omega/\partial p\cdot\delta p = 0$ and the evolution law for the viscoelastic strains as indicated by the dissipation function. The variation of the dissipation function $\delta\Phi$ is to be understood in the same manner as in (21).

5 COMPUTATIONAL RESULTS

All results are computed for polydimethylsiloxane Sylgard184 [11]. The examples are chosen such that not only the capability of the formulation in reproducing standard viscoelastic effects and also electromechanic breakdown is proven, but also with a view to subsequent verification against measurements at a later time. To determine the viscoelastic parameters such as the long-term modulus μ_∞ and the viscous properties μ_i and η_i, measurement data from a small-strain dynamic thermo-mechanical analysis (DTMA) for Sylgard184 are available [6]. From this data, a Prony series representation is fitted by a non-linear, non-negative least squares algorithm. The corresponding material constants are collected in Table 1. The dielectric constant is taken as $\epsilon_r = 2.72$, compare [11].

Table 1: Material parameters used in computations.

i	∞	1	2	3	4
μ_i in $\mathrm{N\,m^{-2}}$	172068.34205	146303.75628	109530.3796	669288.7113	212494.6987
η_i in $\mathrm{N\,s\,m^{-2}}$	-	5041.3227	32822.3631	454.7618	1162.9012

5.1 Circular plate

The first example is a thin circular plate of height $h = 1\,\mathrm{mm}$ and radius $R = 5\,\mathrm{mm}$ and with an assumed density of $\rho_{Syl} = 1000\,\mathrm{kg\,m^{-3}}$. A rotationally symmetric setup is displayed in Figure 2, where no frictional forces are assumed to act on the plate surfaces. Two electrodes are located on the top and bottom of the sample. While the bottom electrode is grounded, an electric potential is applied to the upper electrode. This causes the plate to contract in thickness direction and expand in the plane.

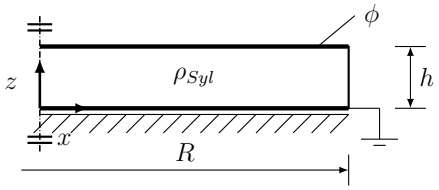

Figure 2: Example 1: Circular plate

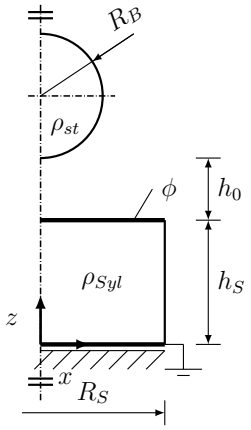

Figure 3: Example 2: Ball-drop

We consider a simulation period of $10\,\mathrm{s}$ in total, where the electric potential is increased linearly up to the given value over the first two seconds, and kept constant afterwards. To avoid numerical damping, we choose $\gamma = 0.5$ and thus $\beta = 0.25$. A total of 10 different voltages are applied consecutively, ranging between $10\,\mathrm{kV}$ and $55\,\mathrm{kV}$. In the left plot of Figure 4 the evolution of the change in thickness due to the applied electric field is visualized. On observes that the change in thickness grows disproportionally as the voltage is increased. This is due to geometric nonlinearities, as a smaller distance between electrodes directly implies a larger electric field. At a voltage of $55\,\mathrm{kV}$, the change in thickness amounts to $u_z = -0.239\,\mathrm{mm}$, which corresponds to a strain of about 24%. Above a certain voltage, the collapse (*breakdown*) of the specimen is observed, compare right plot of Figure 4.

5.2 Ball drop test

As a second example we consider the ball drop experiment. As in Figure 3 shown, we consider a cylindrical specimen made from Sylgard 184 with a radius of $R_S = 30\,\mathrm{mm}$ and a height of $h_S = 30\,\mathrm{mm}$. A steel ball of radius $r_B = 15\,\mathrm{mm}$ and density $\rho_{st} = 7830\,\mathrm{kg\,m^{-3}}$ is to fall onto this specimen from an initial height $h_0 = 500\,\mathrm{mm}$ above the cylinder's surface.

A finite element model exploiting the model's radial symmetry is generated, where the finite element mesh consists of 234 triangular elements. Third order elements are used in simulations, which results in a total of 2314 displacement degrees of freedom. In a first sub-step of the simulation, an electric potential is applied to electrodes located at top and bottom of the cylinder.

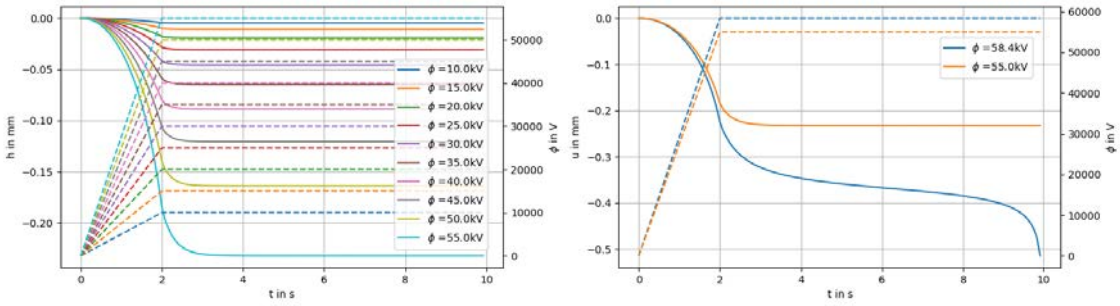

Figure 4: Displacement due to electric potential (left) and electric breakdown, observed for a voltage of $58.4\,\mathrm{kV}$

Table 2: Rebound resilience for different electric loads.

voltage ϕ_0/MV	0	1.00	1.25	1.50
change of height w_1/mm	0	1.77	3.01	4.97
rebound height h_1/mm	174.81	165.32	159.12	148.88
rebound resilience R	0.347	0.328	0.314	0.290

At time $t_0 = 9.4\,\mathrm{s}$, the ball is released. Again, the Newmark parameters are chosen as $\beta = 0.25$ and $\gamma = 0.5$ to avoid numerical damping. Around the expected impact time, the time step size is reduced to $\Delta t = 0.05\,\mathrm{ms}$ to generate accurate results.

Damping properties of the material are often characterized through the rebound resilience or loss factor in the ball drop test, see [7]. The loss factor is given by $\tan\delta = h_1/h_0$, with h_1 the first rebound height. In the current simulation, the effect of an applied electric potential on the rebound resilience is studied.

In the left of Figure 5 the trajectory of the ball center point is displayed, while the right plot shows the vertical displacement of the center point of the top surface of the cylinder due to the applied electric field and the impact of the ball. When no electric field is applied (blue curve), we get a rebound height of $h_1 = 174.81\,\mathrm{mm}$ and therefore a rebound resilience of $R = 34.7\,\%$. After applying electric fields of $1\,\mathrm{MV}$, $1.25\,\mathrm{MV}$ and $1.5\,\mathrm{MV}$ a change in rebound heights is observed. According data is collected in Table 2, where w_1 denotes the absolute change of height of the cylinder due to electric loading. The rebound resilience is then computed as $R = (h_0 + w_1)/(h_1 + w_1)$. The results imply that damping properties can be adapted through electric actuation.

REFERENCES

[1] W. Voigt, *Lehrbuch der Kristallphysik*. BG Teubner, 1910, vol. 34.

[2] G. Maugin, *Continuum Mechanics of Electromagnetic Solids*. North-Holland, 1988.

[3] L. Dorfmann and R. W. Ogden, "Nonlinear electroelasticity: material properties, contin-

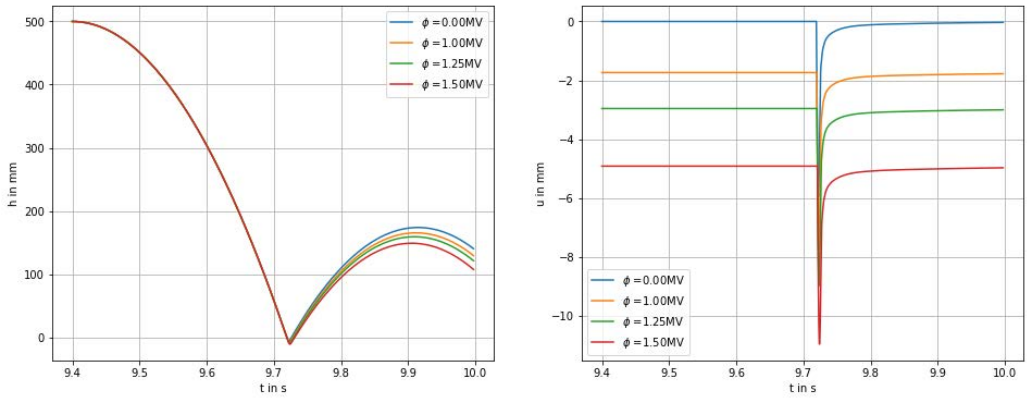

Figure 5: Trajectory of ball during free fall and rebound after contact (left) and vertical displacement of center point on top surface of the specimen due to electric actuation and impact (right)

uum theory and applications," *Proceedings of the Royal Society A: Mathematical, Physical and Engineering Sciences*, vol. 473, no. 2204, p. 20170311, 2017.

[4] A. Ask, A. Menzel, and M. Ristinmaa, "Electrostriction in electro-viscoelastic polymers," *Mechanics of Materials*, vol. 50, pp. 9–21, 2012.

[5] C. Miehe, D. Rosato, and B. Kiefer, "Variational principles in dissipative electro-magneto-mechanics: a framework for the macro-modeling of functional materials," *International Journal for Numerical Methods in Engineering*, vol. 86, no. 10, pp. 1225–1276, 2011.

[6] R. P. Preuer, "Mechanical characterisation of energy dissipation in silicone elastomer blends," 2018, master thesis, Universität Linz.

[7] C. Emminger, U. D. Çakmak, R. Preuer, I. Graz, and Z. Major, "Hyperelastic material parameter determination and numerical study of TPU and PDMS dampers," *Materials*, vol. 14, no. 24, p. 7639, 2021.

[8] P. Haupt, *Continuum Mechanics and Theory of Materials*. Berlin Heidelberg: Springer Science and Business Media, 2013.

[9] I. Doghri, *Mechanics of Deformable Solids - Linear, Nonlinear, Analytical and Computational Aspects*. Berlin Heidelberg: Springer Science and Business Media, 2013.

[10] C. Taylor and P. Hood, "A numerical solution of the Navier-Stokes equations using the finite element technique," *Computers & Fluids*, vol. 1, no. 1, pp. 73–100, 1973.

[11] The Dow Chemical Company. (2017) Sylgard184 datasheet. [Online]. Available: https://www.dow.com/content/dam/dcc/documents/en-us/productdatasheet/11/11-31/11-3184-sylgard-184-elastomer.pdf